Electronic Supplementary Material

# A Fluorene-Carbazole Conjugated Polymer Hole Conductor for Efficient and Stable Perovskite Solar Cells

Bei Wang[a], Junjun Guo[a], Xuanang Luo[b], Chenxu Han[a], Bo Zhao[a], Ihsan Ullah[a], Yuxin Kong[a], Xinyu Zhao[a], Lei Ying[b,*], Jianyu Yuan[a,*]

[a]*Jiangsu Key Laboratory for Carbon-Based Functional Materials & Devices, Institute of Functional Nano & Soft Materials (FUNSOM), Soochow University, 199 Ren'ai Road, Suzhou, 215123 Jiangsu, P. R. China*

[b]*Institute of Polymer Optoelectronic Materials and Devices, State Key Laboratory of Luminescent Materials and Devices, South China University of Technology, 381 Wushan Road, Guangzhou, 510640 Guangdong, P.R. China.*

*Corresponding author: msleiying@scut.edu.cn (L. Y.); jyyuan@suda.edu.cn (J. Y.)

**Materials:**

PF8Cz was prepared and purchased from VOLT-AMP optoelectronics Tech. Co., Ltd, lead bromide ($PbBr_2$, 99.99%) and lead iodide ($PbI_2$, 99.999%) from Sigma-Aldrich, cesium iodide (CsI, 99.99%) was from Alfa Aesar and formamidinium iodide (FAI, 99.9%) and methylammonium bromide (MABr, 99.99%) from Great solar, 2,2',7,7'-tetrakis[N,N-di(4-methoxyphenyl)amino]-9,9'-spirobifluorene (Spiro-OMeTAD), poly[bis(4-phenyl)(2,4,6-trimethyl-phenyl)amine] (PTAA) and tris(pentafluorophenyl)borane (LAD) from Xi'an Polymer Light Technology Corp. Solvents used for perovskite solar cell include anhydrous N,N-dimethylformamide (DMF) and dimethyl sulfoxide (DMSO), chlorobenzene were from Alfa Aesar. All the materials were used directly without further purification. Glass/F-doped tin oxide (FTO) was purchased from Advanced Election Technology Co., Ltd.

**Characterizations and measurements**

The current density-voltage (*J-V*) characteristics of the solar cells were measured using a Keithley 2400 Digital Source Meter and simulated AM 1.5G spectrum at 100 mW/cm$^2$ with a solar simulator (Class AAA, 94023A-U, Newport) in the ambient atmosphere. Before testing, the light intensity of the xenon lamp was calibrated with a standard silicon solar cell (91150 V, Newport Oriel). The external quantum efficiency (EQE) measurement of the solar cells was characterized on a Solar Cell Scan 100 system (Zolix Instruments Co. Ltd.). UV-Vis spectra were recorded on a PerkinElmer model Lambda 750. Steady-state PL data and time-resolved PL spectra were obtained by testing with a FluoroMax-4 spectrofluorometer (HORIBA Scientific) with a 150 W ozone-free xenon lamp laser and an excitation wavelength of 490 nm. Cross-section SEM images were obtained by a Zeiss 500 field in high vacuum mode at 15 kV accelerating voltage. The FTO/$TiO_2$/perovskite/HTMs/$MoO_3$ structure was adopted to perform EIS measurements carried out through a Zahner IM6 electrochemical workstation while applying a bias under open-circuit conditions with a frequency between 1 MHz and 100 Hz

under monochromatic LED (500 nm, 100 mW $cm^{-2}$) light irradiation. Cyclic voltammetry (CV) curves of polymers were obtained using a CHI630E electrochemical workstation with a three-electrode system. The working electrode was a glassy carbon electrode, the reference electrode was a saturated calomel electrode (SCE), and the counter electrode was a platinum wire. The electrolyte solution was 0.1 M tetrabutylammonium hexafluorophosphate ($TBAPF_6$) in anhydrous acetonitrile. The experiments were conducted under a nitrogen atmosphere at a scan rate of 200 mV $s^{-1}$. The energy levels of the highest occupied molecular orbital ($E_{HOMO}$) of the polymers were calculated from the onset oxidation and reduction potentials, respectively, using the following equation: $E_{HOMO} = -\left[e\left(E_{ox} - E_{Fc/Fc+} + 5.1\right)\right] (eV)$, where $e$ is the elementary charge, $E_{ox}$ are the onset oxidation potential versus the calomel electrode, and $E_{Fc/Fc+}$ is the ferrocene/ferrocenium redox potential versus SCE, which was measured as 0.42 V. Grazing incidence wide-angle X-ray scattering (GIWAXS) was performed using MetalJet-D2, Excillum (Xenocs, France). The X-ray wavelength is 0.134144 nm. The sample-to-detector distance was 214.545 mm, and the incidence angle of the X-ray beam to the film surface was set at 0.20°. Scattering images were recorded using a 2D detector (Pilatus3R 1M, Dectris). The resulting GIWAXS data was analyzed using a custom Python-based code.

*TRPL fitting*:

The TRPL test results were fitted by a biexponential function as follows:

$$f(t) = A_1 e^{\left(-\frac{t}{\tau_1}\right)} + A_2 e^{\left(-\frac{t}{\tau_2}\right)} + A_0$$

where $A_0$ is a constant, $t$ is the time, $A_1$ and $A_2$ are the decay amplitudes, $\tau_1$ and $\tau_2$ are the decay times, and the average PL lifetime ($\tau_{ave}$) can be obtained by the following equation:

$$\tau_{ave} = \frac{A_1\tau_1^2 + A_2\tau_2^2}{A_1\tau_1 + A_2\tau_2}$$

*SCLC measurements*:

SCLC measurements are often followed by three regimes: (i) the ohmic region ($I \propto V$) to calculate the electrical conductivity, (ii) the TFL region ($I \propto V^n$, n>2) to estimate the trap density, and (iii) Child's region ($I \propto V^2$) to determine the charge mobility. The *J-V* characteristics of the hole-only devices are fitted using the Mott-Gurney law, expressed as:

$$J = \frac{9}{8}\varepsilon\varepsilon_0\mu\frac{V^2}{L^3}$$

where $\varepsilon$ is the dielectric constant of the active layer, $\mu$ is the mobility, $\varepsilon_0$ is the permittivity of free space, and $L$ is the thickness of the active layer. All measurements were performed in the dark, and the voltage was scanned from -5 to 5 V.

Furthermore, the conductivity ($\sigma$) was extracted from the slope of the current-voltage (*I-V*) curve:

$$I = \frac{\sigma AV}{d}$$

where $A$ is the area of the sample and $d$ is the thickness of the HTMs.

*Trap density*:

A pure hole device of FTO/PEDOT:PSS/Perovskite/HTMs/$MoO_3$/Ag was used to characterize the trap density ($n_{trap}$) in the device. The trap density characterization satisfies the following equation:

$$V_{TFL} = \frac{eL^2}{2\varepsilon_0\varepsilon_r}n_{trap}$$

where $V_{TFL}$ is the trap-filled limit voltage and $L$ is the thickness of the perovskite film.

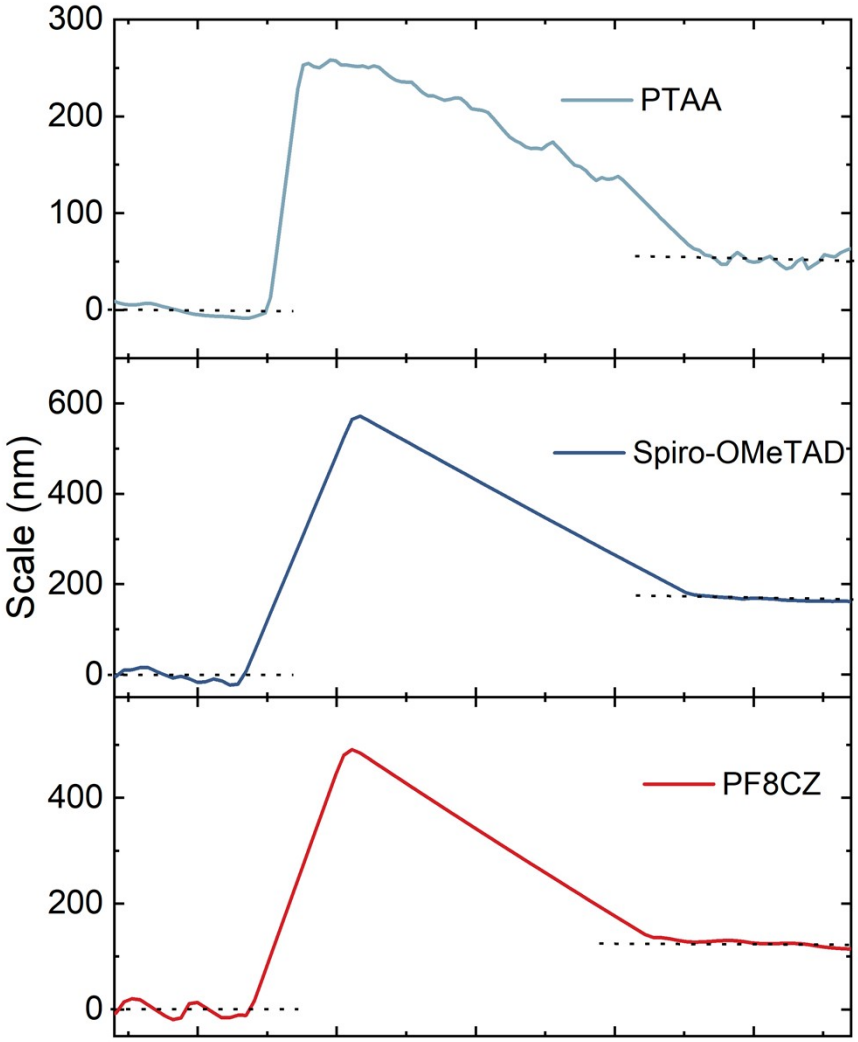


Fig. S1. AFM Step-height profiles for extracting thickness of HTM: ~50 nm (PTAA); ~160 nm (Spiro-OMeTAD); ~120 nm (PF8Cz).

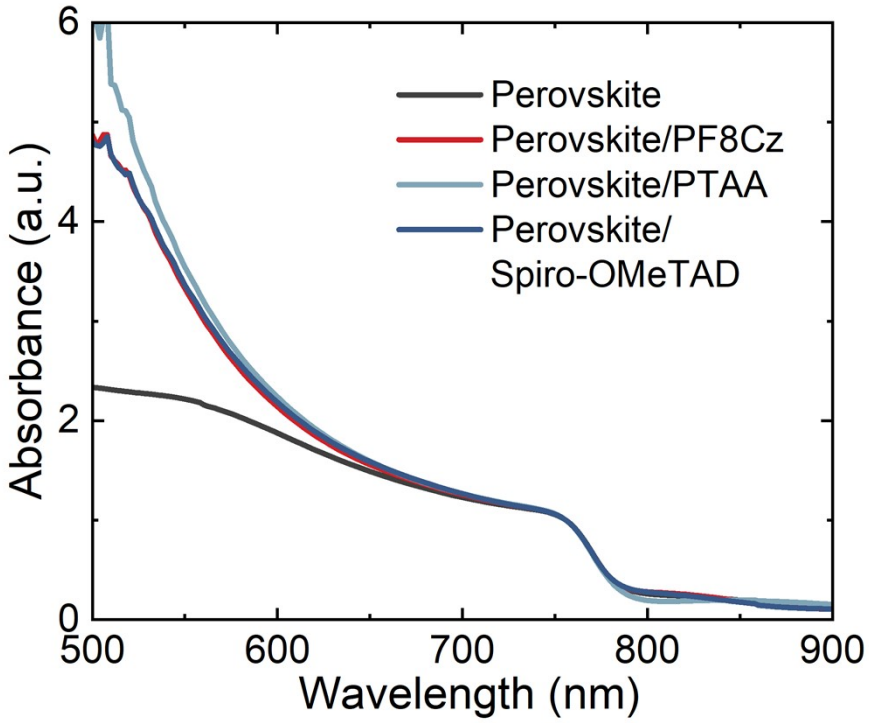


Fig. S2. UV-vis absorption spectra of perovskite and perovskite/different HTMs films.

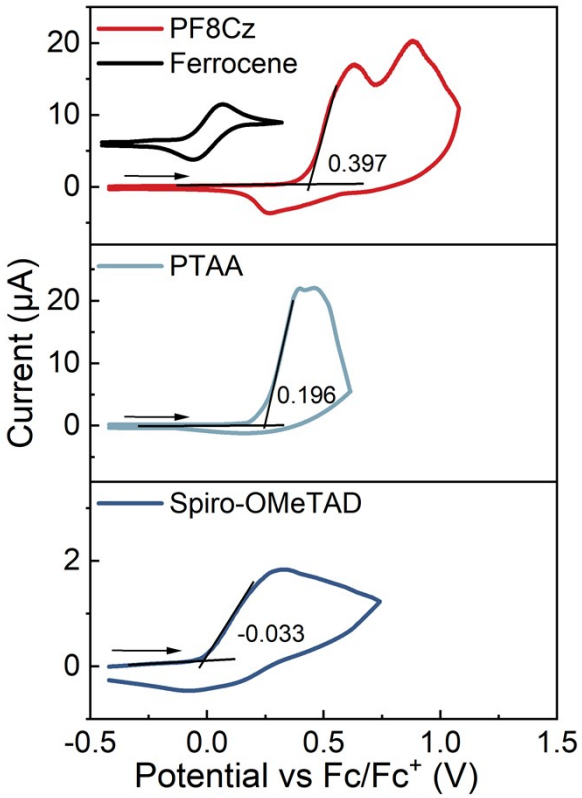


Fig. S3. Cyclic voltammetry curves of the oxidation of films.

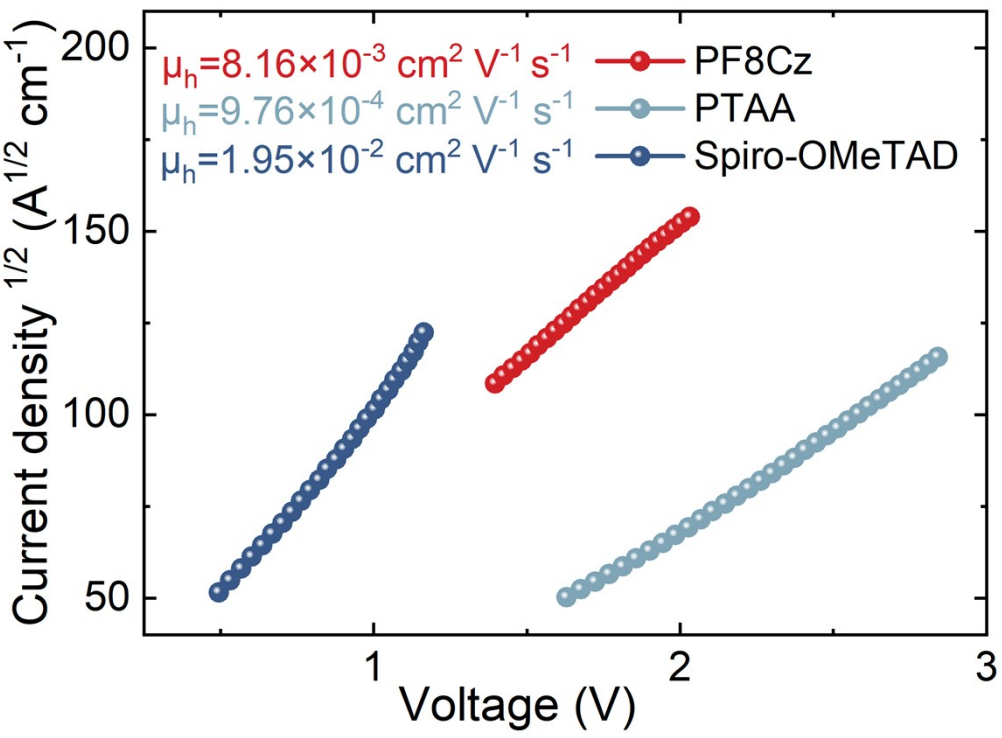


Fig. S4. $J^{1/2}$-$V$ characteristics of the different HTMs based on hole-only devices.

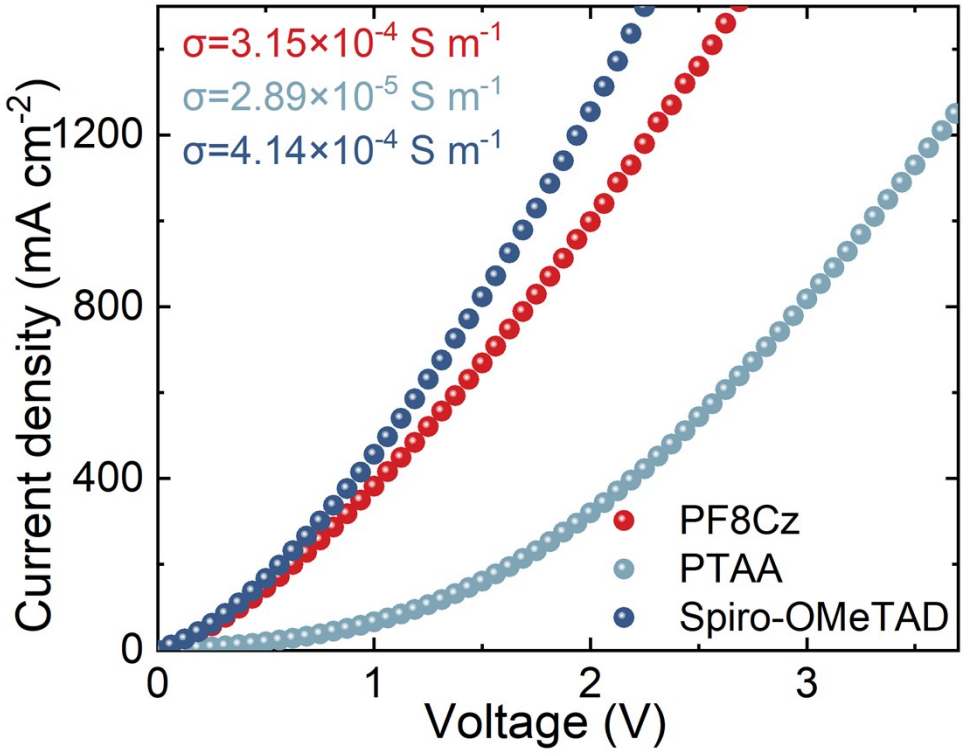


Fig. S5. J-V characteristics of the different HTMs based on hole-only devices.

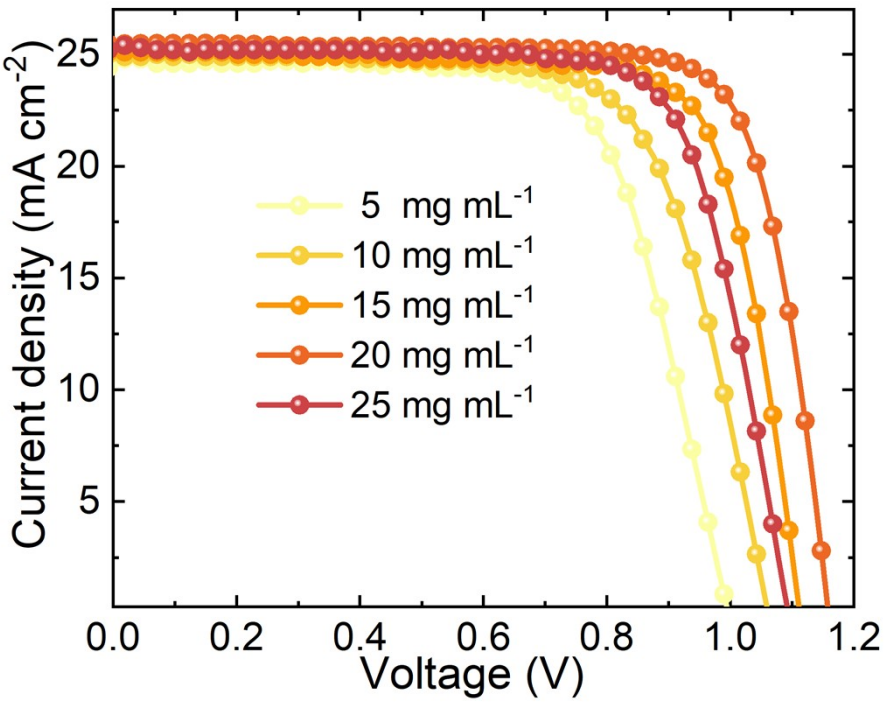


Fig. S6. *J-V* curves based on different concentrations of PF8Cz-based PSCs.

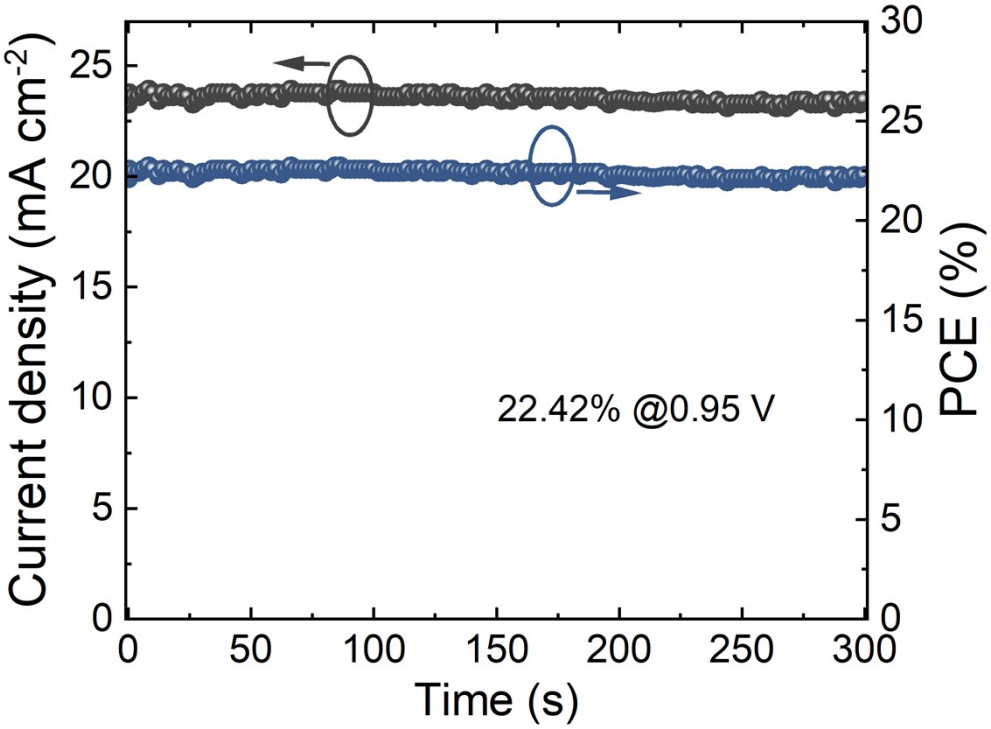


Fig. S7. The SPO of the Spiro-OMeTAD-based PSCs.

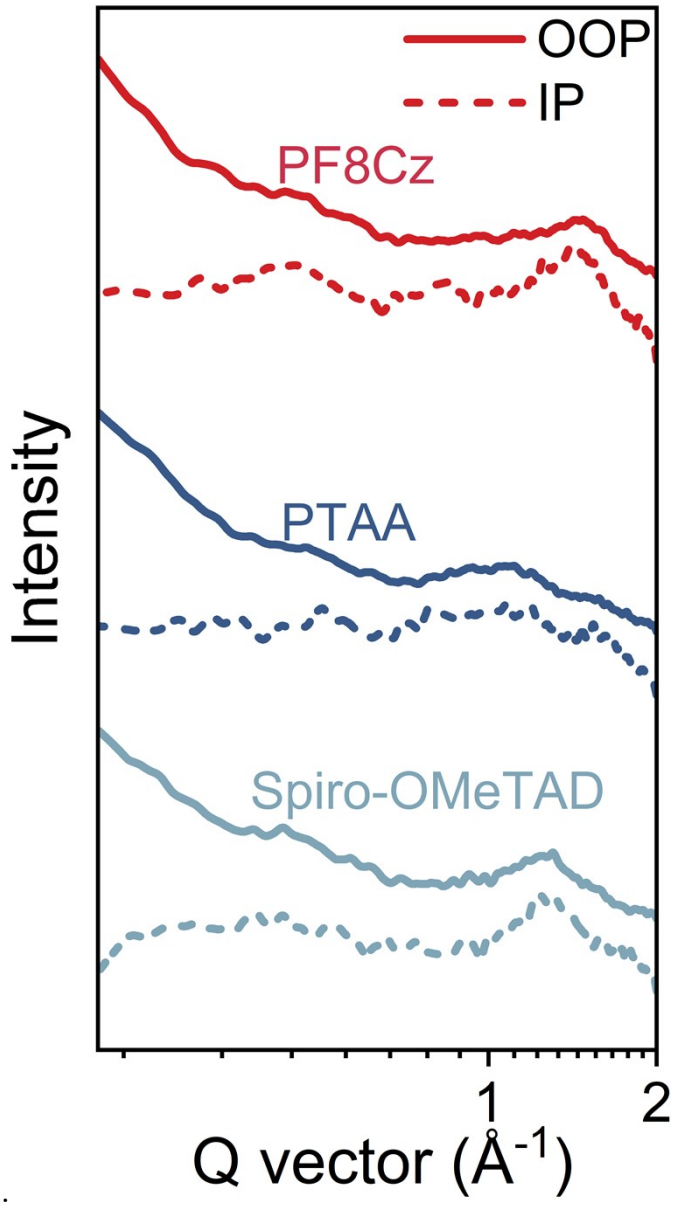


Fig. S8. Sector-averaged *I-q* curves in the IP (dashed lines) and OOP (solid lines) directions.

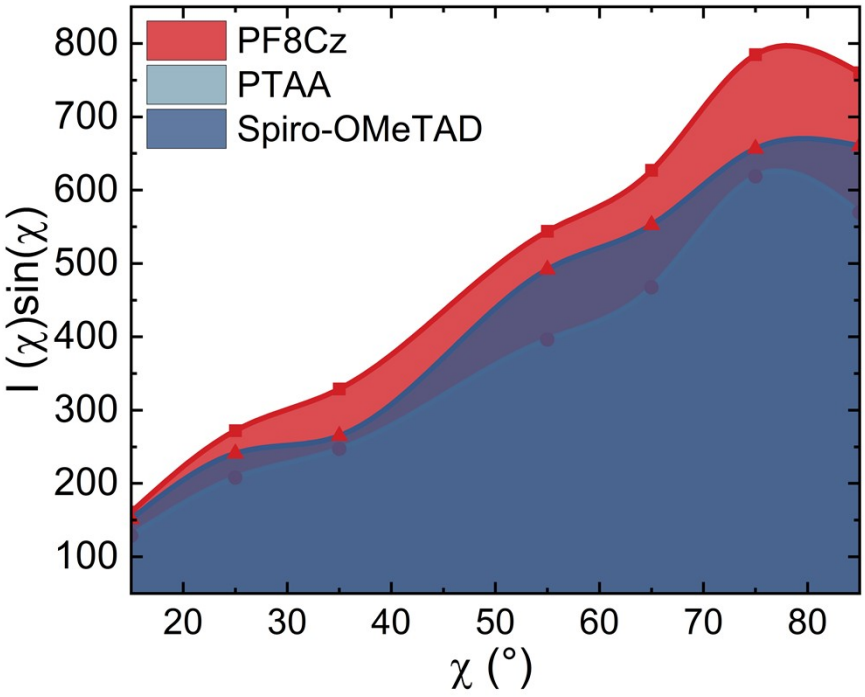


Fig. S9. $Intensity \cdot \sin \chi$ as a function of $\chi$ of PF8Cz, PTAA, and spiro-OMeTAD thin films. Inset are the calculated rDoC values.

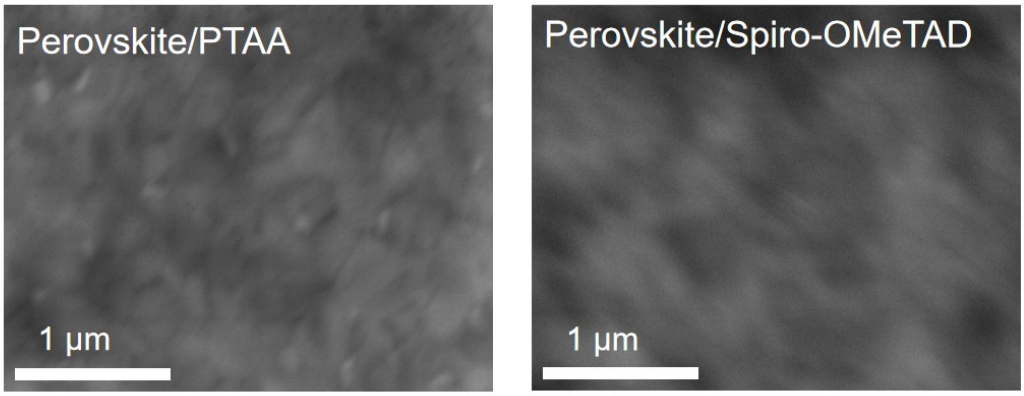


Fig. S10. Top-view SEM images of perovskite/PTAA and perovskite/Spiro-OMeTAD.

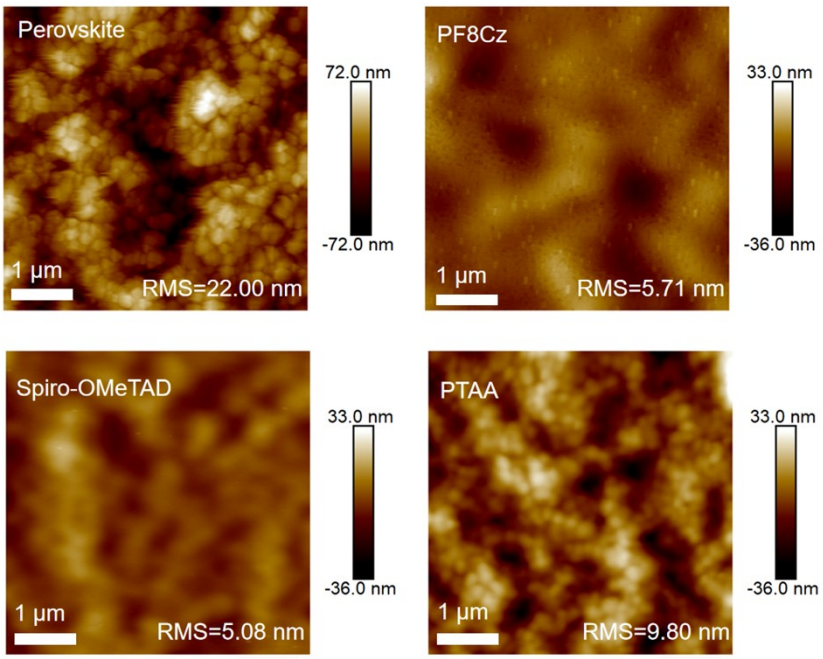


Fig. S11. AFM images of the perovskite and perovskite/different HTMs films.

Table S1. PV device parameters of different concentrations of PF8Cz-based PSCs.

| Condition | $V_{OC}$ (V) | $J_{SC}$ (mA/cm$^2$) | *FF* (%) | PCE (%) |
|---|---|---|---|---|
| 5 mg mL$^{-1}$ | 0.998 | 24.45 | 0.70 | 17.09 |
| 10 mg mL$^{-1}$ | 1.069 | 24.95 | 0.70 | 18.55 |
| 15 mg mL$^{-1}$ | 1.121 | 25.09 | 0.76 | 21.31 |
| 20 mg mL$^{-1}$ | 1.174 | 25.47 | 0.78 | 23.05 |
| 25 mg mL$^{-1}$ | 1.095 | 25.18 | 0.74 | 20.45 |

Table S2. Fitting parameters of the decay amplitude and decay time obtained from TRPL spectra.

| Condition | $\tau_{average}$ (ns) | $\tau_1$ (ns) | $\tau_2$ (ns) | $A_1$ | $A_2$ |
|---|---|---|---|---|---|
| Perovskite | 738.5 | 11.3 | 1026.2 | 570.8 | 15.8 |
| Perovskite/Spiro-OMeTAD | 4.6 | 0.9 | 7.5 | 2276.4 | 330.4 |
| Perovskite/PF8Cz | 11.6 | 0.8 | 15.1 | 1623.4 | 259.3 |

| | | | | | |
|---|---|---|---|---|---|
| Perovskite/PTAA | 23.1 | 4.5 | 41.9 | 929.8 | 100.1 |

Table S3. Recently reported n-i-p PSCs based on conjugated polymer HTM with > 22% effici

| HTMs | Device architectures | PCE (%) | References |
|---|---|---|---|
| PT-Cz50 | ITO/SnO2/PVSK/HTM/$MoO_3$/Ag | 22.53% | *Adv. Funct. Mater*., 2023, **33**, 2308435 |
| PC-DPP | TO/SnO2/perovskite/HTMs/$MoO_3$/ Ag | 22.67%. | *ACS Energy Lett*., 2023, **8**, 2878 |
| PFBTI | glass/ITO/$SnO_2$/$Cs_{0.05}FA_{0.95}PbI_3$/H TM/$MoO_3$/Ag | 23.10% | *Adv. Mater.,* 2022, **34**, 2110587 |
| PM6 | ITO/$SnO_2$/perovskite/HTMs/$MoO_3$/ Ag | 24.04%, | *Angew. Chem. Int. Ed.,* 2022, **61**,e202210356 |
| PE10 | lass/ITO/$SnO_2$/perovskite ($FA_{0.85}MA_{0.15}PbI_3$)/HTM/$MoO_3$/Ag | 22.30% | *Angew. Chem. Int. Ed.,* 2022, **61**, e202201847 |
| Nap-SiBTA | FTO/compact-$TiO_2$/mesoporous-$TiO_2$/perovskite/NapSiBTA or Spiro-OMeTAD/Au | 23.07% | *Adv. Energy Mater*., 2023, **13**, 2202680 |
| PTTDZ-Cl | FTO/$SnO_2$/FAMA perovskite/HTM/$MoO_3$/Ag. | 22.20% | *Sol. Rrl,* 2023, 2300706 |
| PNTDT-2F2T | ITO/$SnO_2$/$MAPbI_3$/HTM/Au. | 22.19% | *J. Mater. Chem.a,* 2022, **10**, 12187 |
| PBQ6 | ITO/$SnO_2$/perovskite/polymer HTM/$MoO_3$/Ag | 22.60% | *Science China Chemistry,* 2021, **64**, 2035 |
| PC6 | glass/FTO/$SnO_2$/perovskite ($MAPbI_3$)/HTM/Au | 22.20% | *Angew.Chem.Int.Ed.,* 2022, **61**, e202114341 |
| 2DP-TDB | ITO/$SnO_2$/$FA_{0.85}MA_{0.15}PbI_3$/HTMs/ $MoO_3$/Ag | 22.17% | *ACS Energy Lett.,* 2021, **6**, 1521 |
| PBTFO | ITO/$SnO_2$/perovskite/polymer HTM/Au | 22.10% | *Nano Energy,* 2020, **78**, 105159 |
| PBDB-Cz | ITO/$SnO_2$/perovskite/HTM/$MoO_3$/ Ag | 22.06% | *Adv. Energy Mater.,* 2022, **12**, 2102697 |
| **PMSe** | ITO/SnO2/perovskite/HTMs/$MoO_3$ /Ag | 24.53% | *J. Am. Chem. Soc.,* 2022, **144**, 9500 |
| **PFBCz** | **ITO/$TiO_2$/perovskite/HTM/$MoO_3$ /Ag** | **23.28%** | **This work** |